

Star formation history and X-ray binary populations: the case of the Small Magellanic Cloud

V. Antoniou^{1,2,3}, A. Zezas^{1,2,4}, D. Hatzidimitriou^{4,5}, V. Kalogera⁶

ABSTRACT

Using *Chandra*, *XMM-Newton* and optical photometric catalogs we study the young X-ray binary (XRB) populations of the Small Magellanic Cloud. We find that the Be/X-ray binaries (Be-XRBs) are observed in regions with star formation rate bursts ~ 25 -60 Myr ago. The similarity of this age with the age of maximum occurrence of the Be phenomenon (~ 40 Myr) indicates that the presence of a circumstellar decretion disk plays a significant role in the number of observed XRBs in the 10-100 Myr age range. We also find that regions with strong but more recent star formation (e.g., the Wing) are deficient in Be-XRBs. By correlating the number of observed Be-XRBs with the formation rate of their parent populations, we measure a Be-XRB production rate of ~ 1 system per $3 \times 10^{-3} M_{\odot}$ /yr. Finally, we use the strong localization of the Be-XRB systems in order to set limits on the kicks imparted on the neutron star during the supernova explosion.

Subject headings: Magellanic Clouds—pulsars: general—stars: early-type—stars: emission-line, Be—stars: formation—X-rays: binaries

¹Harvard-Smithsonian Center for Astrophysics, 60 Garden Street, Cambridge, MA 02138, USA; vantonio@head.cfa.harvard.edu

²Physics Department, University of Crete, P.O. Box 2208, GR-710 03, Heraklion, Crete, Greece

³Department of Physics and Astronomy, Iowa State University, 12 Physics Hall, Ames, IA 50011, USA

⁴IESL/Foundation for Research and Technology-Hellas, P.O. Box 1527, GR-711 10 Heraklion, Crete, Greece

⁵Section of Astrophysics, Astronomy and Mechanics, Department of Physics, University of Athens, Panepistimiopolis, GR-157 84 Zografos, Athens, Greece

⁶Department of Physics and Astronomy, Northwestern University, 2145 Sheridan Road, Evanston, IL 60208, USA

1. Introduction

Nearby star-forming galaxies offer a unique environment to study the young (<100 Myr) X-ray binary (XRB) populations. One of the best cases is the Small Magellanic Cloud (SMC), which at ~ 60 kpc is our second nearest star-forming galaxy (Hilditch et al. 2005). Its proximity, well mapped extinction (Zaritsky et al. 2002), moderate Galactic foreground absorption ($N_{\text{H}} \simeq 6 \times 10^{20} \text{cm}^{-2}$; Dickey & Lockman 1990), small line-of-sight depth of its young, central stellar populations (<10 kpc; Crowl et al. 2001; Harries et al. 2003), and its well-determined recent star formation history (SFH; Harris & Zaritsky 2004 [HZ04]) make the SMC the ideal environment for directly studying the link between XRB populations and star formation (SF). Furthermore, the wealth of multi-wavelength data allows us to clarify the X-ray sources and obtain an even more precise picture of their population.

Several studies have compared the number of Be/X-ray binaries (Be-XRBs) in the Magellanic Clouds and the Galaxy (e.g., Majid et al. 2004, Haberl & Pietsch 2004, Coe et al. 2005), concluding that the SMC hosts an unusually large number of these systems. There is only one identified supergiant XRB located in the SMC Wing (SMC X-1; Webster et al. 1972) in a population of ~ 100 High-Mass XRBs (HMXBs; e.g., Liu et al. 2005, Antoniou et al. 2009b [Paper II]). However, only few of those HMXBs have determined spectral types (e.g., out of the 92 listed in Liu et al. 2005, 53 are cited as Be-XRBs but only 19 have been confirmed spectroscopically). Later works by Antoniou et al. (2009a [Paper I]), Haberl et al. (2008), McBride et al. (2008), Shtykovskiy & Gilfanov (2005), Coe et al. (2005) and others have increased the number of known Be-XRBs to 67 to date. Nevertheless, this overabundance can be partly explained by the enhanced SMC SFH ~ 40 Myr ago (e.g., Majid et al. 2004, Shtykovskiy & Gilfanov 2007 [SG07]). However, Antoniou et al. (2009b) show that even after accounting for the difference in the star formation rate (SFR) between the SMC and the Galaxy, the SMC hosts ~ 1.5 times more Be-XRBs than the Galaxy down to a limiting luminosity of $L_{\text{X}} \geq 10^{34} \text{erg s}^{-1}$. This residual excess can be explained by the different metallicity of these galaxies, as justified by population synthesis models (Dray 2006) and recent observations of Be stars (e.g., Wisniewski & Bjorkman 2006, Martayan et al. 2007). The work of Antoniou et al. (2009b) also indicated spatial variations of the Be-XRB populations within the SMC Bar, which could be evidence for small supernova (SN) kicks.

The SMC Bar hosts stellar populations with ages <100 Myr [HZ04] and the vast majority of the SMC pulsars (Galache et al. 2008). [SG07] found that the age distribution of the HMXBs peaks at ~ 20 -50 Myr after the SF event, while McSwain and Gies (2005) observed a strong evolution in the fraction of Be stars with age up to 100 Myr, with a maximum at ~ 25 -80 Myr. These results motivated us to investigate the connection between the spatially resolved SFH in and around the SMC Bar and the number and spatial distribution of the

XRBs. In this study, we use the results from our *Chandra* survey of the central, most actively star forming, SMC Bar (A. Zezas et al. 2010, in preparation; Papers I, II), and data from our *XMM-Newton* survey of the outer SMC regions which host young and intermediate age stellar populations (~ 10 -500 Myr; [HZ04]).

2. X-ray observations and data analysis

Using the ACIS-I detector on board *Chandra* we observed five fields in the central part of the SMC (the so called SMC Bar), with typical exposure times of 8-12 ks. These observations yielded a total of 158 sources, down to a limiting luminosity of $\sim 4 \times 10^{33}$ erg s $^{-1}$ (0.5-7.0 keV band), reaching the luminosity range of quiescent HMXBs (typically $L_X \sim 10^{33} - 10^{35}$ erg s $^{-1}$; van Paradijs & McClintock 1995). The analysis of the data, the source-list and their X-ray luminosity functions are presented in A. Zezas et al. (2010, in preparation), while their optical counterparts and resulting classification are given in Papers I, II.

Our *XMM-Newton* survey consists of five observations in the outer SMC Bar, performed with the three EPIC (MOS1, MOS2, and PN) detectors in full frame mode. One of these fields was affected by high background flares and it is not included in this work. The data were analyzed with the *XMM-Newton* Science Analysis System (SAS) version 7.0.0. After processing the raw data with the *epchain* and *emchain* tasks, we filtered any bad columns/pixels and high background flares (excluding times when the total count rate deviated more than 3σ from the mean), resulting in 5-18 ks net exposures. We only kept events of patterns 0-4 for the PN and 0-12 for the MOS detectors. Source detection was performed simultaneously in five energy bands (0.2-0.5, 0.5-1.0, 1.0-2.0, 2.0-4.5, and 4.5-12.0 keV), and the three EPIC detectors with the maximum likelihood method (threshold set to 7) of the *edetect_chain* task. The detected sources were visually inspected for spurious detections. We detected 186 sources down to a limiting luminosity of $\sim 3.5 \times 10^{33}$ erg s $^{-1}$ (0.2-12 keV), out of which 4-8 sources are expected to be spurious based on the calibration of Watson et al. (2009).

In Table 1, we give the ID and the coordinates of the X-ray fields, along with the properties of the dominant SF event in each field (see §3).

2.1. X-ray source classification

New HMXBs and candidate Be-XRBs are identified based on their X-ray and optical properties. Hardness ratios between the soft (0.5-1.0 keV), medium (1.0-2.0 keV), and hard (2.0-4.5 keV) bands were used as an initial measurement of their X-ray spectral properties.

A hard X-ray spectrum or hardness ratio (equivalent to a photon index of $\Gamma \sim 1$) is indicative of a pulsar binary (e.g., Haberl et al. 2008). For the identification of the optical counterparts of the *XMM-Newton* sources we followed the analysis of Antoniou et al. (2009b). We cross-correlated their coordinates with the OGLE-II (Udalski et al. 1998) and MCPS (Zaritsky et al. 2002) catalogs, and searched for optical matches in a $5''$ radius around each X-ray source (which includes the boresight error of *XMM-Newton*; e.g., Brusa et al. 2007). Given the small number of X-ray sources with independently known optical counterparts, we cannot correct these observations for boresight errors. Based on the position of these counterparts on the $V, B - V$ color-magnitude diagram, we identify sources with early OB-type counterparts, while from hardness ratio or spectral analysis we identified those hard X-ray sources ($\Gamma \sim 1$), strongly suggesting they are XRB pulsars. Although Monte-Carlo simulations indicate a significant number of spurious sources in these fields, the identification of a hard X-ray source with an early-type counterpart suggests that this is a true match.

We find that 15 *XMM-Newton* sources have O- or B-type counterparts, while only 8 of those are hard X-ray sources, suggesting they are HMXBs. Since all but one of the confirmed SMC HMXBs are Be-XRBs, they are also candidate Be-XRBs. Their properties are presented in Table 2. The X-ray luminosity is derived assuming a power-law spectrum of $\Gamma = 1$ and H I column density equal to 4.81, 6.63, and $4.51 \times 10^{20} \text{ cm}^{-2}$ for fields 1, 2, and 3, respectively (based on Dickey & Lockman 1990). The X-ray spectra of two sources with >200 counts were fitted with an absorbed power law, resulting in a photon index of $\Gamma = 0.65 \pm 0.04$ and 0.97 ± 0.25 , and a column density of $N_{\text{H}} = (3.31 \pm 0.02) \times 10^{20} \text{ cm}^{-2}$ and $(0.30 \pm 0.15) \times 10^{22} \text{ cm}^{-2}$, for sources 2-1 (by simultaneously fitting its MOS1 and MOS2 spectra) and 3-1 (from its PN spectrum), respectively. Source 2-1 in particular is a known Be-XRB pulsar with a period of 169.3 s (Lochner et al. 1998) associated with emission-line object [MA93]623 (Meyssonnier & Azzopardi 1993; $3.3''$ away), source 3-1 remained unclassified in Sasaki et al. 2000 (ROSAT HRI src ID 11), while source 3-3 is the only one not included in the pipeline EPIC detection list.

If we include to the above sources the confirmed and candidate Be-XRBs that lie within the *Chandra* and *XMM-Newton* fields (from this work and those mentioned in §1), we have a total of 54 (39) and 11 (2) HMXBs (Be-XRBs), respectively. For *Chandra* fields this is the sum of unique Be-XRBs, i.e., sources detected in two overlapping fields are counted once.

3. SFH and XRB populations

The recent SFH in our *Chandra* and *XMM-Newton* fields is derived by averaging the spatially resolved SFH of the MCPS regions ($\sim 12' \times 12'$; [HZ04]) encompassed by them.

We find that:

(i) For the *Chandra* fields, the most recent major burst peaked ~ 42 Myr ago, and it had a duration of ~ 40 Myr. Moreover, there were older SF episodes (~ 0.4 Gyr ago) with lower intensity but longer duration, besides a more recent episode (~ 7 Myr) observed only in *Chandra* field 4.

(ii) For *XMM-Newton* field 3, the most recent major burst occurred ~ 67 Myr ago. We also observed two fields with very young populations (most recent major burst at ~ 11 and 17 Myr ago for fields 1 and 2, respectively). *XMM-Newton* field 2 had an additional intense burst ~ 67 Myr ago (Table 1).

In order to investigate the link between stellar and XRB populations, we calculate the average SFH for the MCPS regions ($\sim 12' \times 12'$; [HZ04]) that host one or more Be-XRBs (candidate and confirmed) detected in our *Chandra* and *XMM-Newton* surveys (39 and 2, respectively; see §2.1). The SFH in each region is weighted by the encompassed number of Be-XRBs, and the error bars are derived based on the upper and lower limits of [HZ04]. We repeat this exercise for the 15 MCPS regions without any known Be-XRB in our surveys. The two SFHs are presented in Figure 1. The SFH of the Be-XRBs (black points) is strongly peaked at ~ 42 Myr, while fields without any Be-XRB (gray points) have minimal SFR at this age. This underscores the difference between the fields with and without Be-XRBs, and suggests a clear connection between an SF event and the observed Be-XRBs.

Following the above comparison, we also construct the SFH of the MCPS regions hosting one or more known X-ray pulsars within any of our fields¹ (Figure 1; black points), and for those that do not host such sources (gray points). A large fraction of these pulsars ($\sim 60\%$; Liu et al. 2005) also appears in the Be-XRBs sample, since the vast majority of their companions are Be stars. This link is reinforced by the fact that all the counterparts of these X-ray sources lie on the region of the color-magnitude diagram consistent with main-sequence stars of age ~ 40 Myr (Paper II). For completeness we present both, since the pulsar and the Be-XRB samples are selected on the basis of their timing and optical properties, respectively. In total, in the MCPS regions that overlap with the *Chandra* fields lie 30 X-ray pulsars, while in the *XMM-Newton* fields only 2 (sum of unique sources as in Section 2.1). As expected, the pattern in their SFH is very similar to that of Be-XRBs. For regions rich in X-ray pulsars the SF peaks at ~ 42 Myr, while for regions without pulsars there is no peak at this age.

The average SFH of the MCPS regions with and without any Be-XRBs detected in the

¹Based on the on-line census of Malcolm Coe (<http://www.astro.soton.ac.uk/~mjc/smc/> as of 2009 June 18).

Chandra Wing survey (P.I. M. Coe; McGowan et al. 2008) is presented in Figure 1, top right (black and gray points, respectively). This survey covered 20 fields (3 of which are not used in this study because they do not overlap with any MCPS region), and discovered 4 Be-XRB pulsars (Schurch et al. 2007). Repeating the same analysis, we find an SF peak at ~ 42 Myr for fields with one or more known Be-XRBs. For regions in the Wing without Be-XRBs there is no SF burst at this age; however, we see an intense burst at ~ 11 Myr. For completeness, we also present (Figure 1) the average SFH of the MCPS regions with candidate (i.e., non spectroscopically confirmed) Be-XRBs from the census of Liu et al. (2005), which also shows that they are produced from the same SF burst as the pulsars and confirmed Be-XRBs. The above comparisons are summarized in Table 3.

The strong correlation between the number of XRBs and the age of the stellar populations at their location allows us to measure for the first time the XRB formation rate per unit SFR of their *parent* populations. The number of Be-XRBs (or HMXBs) per unit area detected in our *Chandra* and *XMM-Newton* surveys versus the SFR at ~ 42 Myr for the different fields is plotted in Figure 2. In order to have a homogenous sample we used Be-XRBs detected only in these surveys. The best fit bisector line was calculated using the “Linear Regression Software” (Akritas & Bershadsky 1996), which takes into account heteroscedastic errors. We find a slope of 0.35 ± 0.03 Be-XRBs/SFR (or 0.40 ± 0.04 HMXBs/SFR), where SFR is in units of $10^{-3} M_{\odot}/\text{yr}$. This is the first direct calibration of the XRB formation rate and the fact that it is based on the source population in a single galaxy minimizes systematic effects related to metallicity. For the same reason, this reflects the Be-XRB formation rate for a low metallicity ($\sim 1/5Z_{\odot}$; Luck et al. 1998).

4. Discussion

From the above analysis we find that the number of SMC XRBs peaks for stellar populations of ages ~ 25 -60 Myr. In Figure 1, we also see two additional peaks at ~ 11 and ~ 422 Myr. The one at ~ 11 Myr is too early to produce any pulsar XRBs, but could result in a population of black-hole binaries (Belczynski et al. 2008) with O or early B-type donors which due to their massive companion evolve fast. The second SFR peak (at ~ 422 Myr) cannot result in HMXB formation, since by that time all OB stars have ended their lives.

The large number of Be-XRBs observed at ages ~ 25 -60 Myr is consistent with the work of McSwain & Gies (2005), who find that Be stars develop their decretion disks at ages of ~ 25 -80 Myr, with a peak at ~ 40 Myr. OB stars formed ~ 40 Myr ago are expected to reach the maximum rate of decretion disk formation at the current epoch.

A study of the evolution of XRBs by [SG07] also found their maximum number at ages of 20-50 Myr after the SF event, which however does not account for the Be phenomenon. They interpret this peak in the HMXB numbers as the result of (1) the pulsar spin-period evolution, (2) the nuclear evolution of the binary system, and (3) the luminosity cutoff ($L_X \sim 10^{34}$ erg s^{-1}) due to the sensitivity of the observations. However, the luminosity cutoff (e.g., Linden et al. 2009) and evolution of the binary system may well result in variations of the observed number of binaries at different ages.

Another factor which may result in the excess of SMC HMXBs stems from the similarity between the epoch of the maximum occurrence of Be stars and the ages of the stellar populations hosting XRBs, and the fact their majority have Be-star donors. This indicates that the development of a decretion disk plays a major role in the overall statistics of the X-ray source populations by (1) increasing the number of active objects and (2) by increasing their observed luminosities due to the higher density and lower velocity of the outflow (Waters et al. 1988).

This is also supported by the deficit of Be-XRBs in the SMC Wing. Figure 1 shows that the Wing has a weaker SF burst at the age of enhanced formation of Be stars (i.e., at ~ 42 Myr) than the Bar, while its most recent SF burst occurred only ~ 11 Myr ago. Thus, based on the above scenario, we do not expect a significant number of SMC Wing Be-XRBs. Indeed, the number of observed sources is lower than that in the SMC Bar, but consistent if we account for the SFR difference at 42 Myr (Figure 2). On the other hand, an SF burst at these early ages (~ 11 Myr ago) suggests that supergiant HMXBs should dominate over Be-XRBs in the Wing. We also note that by comparing the number of binaries against the SFR (or the number of stars) in the same region any projection effects cancel out.

The strong correlation between the number of XRBs and the localized SF event can be used to constrain the kick velocity (v_{kick}) imparted on the compact object during the SN explosion. In the case of large kicks the XRBs would be scattered over larger scales, diluting the correlation with their parent stellar populations and resulting in lower contrast between the SFR of regions with and without XRBs. Given an SF burst at ~ 42 Myr and assuming a minimum pulsar birth timescale of ~ 10 Myr after the burst (e.g., Belczynski et al. 2008), the elapsed time since the kick is ~ 30 Myr. In order to contain the XRBs within the spatial scale of the star-forming regions ($\sim 40'$; [HZ04]), we require a maximum velocity of ~ 15 - 20 km s^{-1} . This is in agreement with measured velocities of Be-XRBs in the Galaxy (15 ± 6 km s^{-1} ; van den Heuvel et al. 2000) and estimations derived from the mean distance between a few pulsars and their nearest clusters in the SMC (~ 30 km s^{-1} ; Coe 2005b). Although these center of mass velocities are consistent with typical SN kicks of ~ 100 km s^{-1} (Cordes & Chernoff 1998), they could be much smaller given that the XRBs show indication

of local concentrations within the Bar associated with SFR enhancements in much smaller scales ($\sim 10'$ - $15'$; Paper II). This suggests at least a factor of two lower v_{kick} which would be consistent with enhanced fraction of electron-capture SNe, which impart very low v_{kick} , as predicted by Linden et al. (2009) for the SMC metallicity.

In this Letter, we discuss the importance of Be-XRBs as a dominant component of young XRBs, based on a study of the connection between X-ray source populations and their parent stellar populations. We find that a significant number of Be-XRBs and/or pulsars are connected with a burst of SF ~ 25 - 60 Myr ago, while regions with weak SFR at ~ 42 Myr, such as the SMC Wing, are deficient in Be-XRBs. We argue that the very strong similarity between the age of maximum occurrence of Be stars and the age of the parent populations of XRBs in the SMC indicates that the Be phenomenon plays a significant role in the number of XRBs in this age range. Finally, based on the spatial correlation between the SF activity and the XRBs, we set a limit on their v_{kick} of ~ 15 - 20 km s $^{-1}$ while there is strong indication for velocities of even a factor of two lower, and we estimate a Be-XRB production rate of ~ 1 system per $3 \times 10^{-3} M_{\odot}$ /yr.

We thank Ewan O’Sullivan for helping with the *XMM-Newton* data analysis, and the anonymous referee for comments which improved this Letter. This work was supported by NASA LTSA grant NAG5-13056, NASA grants G02-3117X, NNX08AB68G, NNG06GE68G, NNX10AH47G, and FP7 grant 206469 (ASTROSPACE).

REFERENCES

- Akritas, M. G., & Bershadsky, M. A. 1996, ApJ, 470, 706
- Antoniou, V., Hatzidimitriou, D., Zezas, A., & Reig, P. 2009a, ApJ, 707, 1080 (Paper I)
- Antoniou, V., Zezas, A., Hatzidimitriou, D., & McDowell, J. C. 2009b, ApJ, 697, 1695 (Paper II)
- Belczynski, K., Kalogera, V., Rasio, F. A., Taam, R. E., Zezas, A., Bulik, T., Maccarone, T. J., & Ivanova, N. 2008, ApJS, 174, 223
- Brusa, M., et al. 2007, ApJS, 172, 353
- Coe, M. J. 2005, MNRAS, 358, 1379
- Coe, M. J., Edge, W. R. T., Galache, J. L., & McBride, V. A. 2005, MNRAS, 356, 502

- Cordes, J. M., & Chernoff, D. F. 1998, *ApJ*, 505, 315
- Crowl, H. H., Sarajedini, A., Piatti, A. E., Geisler, D., Bica, E., Clariá, J. J., & Santos, J. F. C., Jr. 2001, *AJ*, 122, 220
- Dickey, J. M., & Lockman, F. J. 1990, *ARA&A*, 28, 215
- Dray, L. M. 2006, *MNRAS*, 370, 2079
- Galache, J. L., Corbet, R. H. D., Coe, M. J., Laycock, S., Schurch, M. P. E., Markwardt, C., Marshall, F. E., & Lochner, J. 2008, *ApJS*, 177, 189
- Haberl, F., Eger, P., & Pietsch, W. 2008, *A&A*, 489, 327
- Haberl, F., & Pietsch, W. 2004, *A&A*, 414, 667
- Harries, T. J., Hilditch, R. W., & Howarth, I. D. 2003, *MNRAS*, 339, 157
- Harris, J., & Zaritsky, D. 2004, *AJ*, 127, 1531
- Hilditch, R. W., Howarth, I. D., & Harries, T. J. 2005, *MNRAS*, 357, 304
- Linden, T., Sepinsky, J. F., Kalogera, V., & Belczynski, K. 2009, *ApJ*, 699, 1573
- Liu, Q. Z., van Paradijs, J., & van den Heuvel, E. P. J. 2005, *A&A*, 442, 1135
- Lochner, J. C., Marshall, F. E., Whitlock, L. A., & Brandt, N. 1998, *IAU Circ.*, 6814, 1
- Luck, R. E., Moffett, T. J., Barnes, T. G., III, & Gieren, W. P. 1998, *AJ*, 115, 605
- Majid, W. A., Lamb, R. C., & Macomb, D. J. 2004, *ApJ*, 609, 133
- Martayan, C., Frémat, Y., Hubert, A.-M., Floquet, M., Zorec, J., & Neiner, C. 2007, *A&A*, 462, 683
- McBride, V. A., Coe, M. J., Negueruela, I., Schurch, M. P. E., & McGowan, K. E. 2008, *MNRAS*, 388, 1198
- McGowan, K. E., et al. 2008, *MNRAS*, 383, 330
- McSwain, M. V., & Gies, D. R. 2005, *ApJS*, 161, 118
- Meyssonier, N., & Azzopardi, M. 1993, *A&AS*, 102, 451
- Sasaki, M., Haberl, F., & Pietsch, W. 2000, *A&AS*, 147, 75

- Schurch, M. P. E., et al. 2007, MNRAS, 381, 1561
- Shtykovskiy, P., & Gilfanov, M. 2005, MNRAS, 362, 879
- Shtykovskiy, P. E., & Gilfanov, M. R. 2007, Astron. Lett., 33, 437
- Udalski, A., Szymanski, M., Kubiak, M., Pietrzynski, G., Wozniak, P., & Zebrun, K. 1998, Acta Astron., 48, 147
- van den Heuvel, E. P. J., Portegies Zwart, S. F., Bhattacharya, D., & Kaper, L. 2000, A&A, 364, 563
- van Paradijs, J., & McClintock, J. E. 1995, X-ray Binaries, eds. W.H.G. Lewin, J. van Paradijs, and E.P.J. van den Heuvel (Cambridge: Cambridge Univ. Press), p. 58, 58
- Waters, L. B. F. M., van den Heuvel, E. P. J., Taylor, A. R., Habets, G. M. H. J., & Persi, P. 1988, A&A, 198, 200
- Watson, M. G., et al. 2009, A&A, 493, 339
- Webster, B. L., Martin, W. L., Feast, M. W., & Andrews, P. J. 1972, Nature, 240, 183
- Wisniewski, J. P., & Bjorkman, K. S. 2006, ApJ, 652, 458
- Zaritsky, D., Harris, J., Thompson, I. B., Grebel, E. K., & Massey, P. 2002, AJ, 123, 855

Table 1. SFH and HMXB numbers

| ID | Fields | | Age (Myr) | Dominant SF Burst | | Number | | |
|---------------------|--------------------------|--------------------------|--------------|-------------------|--|-----------------|----------|---------|
| | R.A.(J2000.0) (h m s) | Dec.(J2000.0) (° ' ") | | Duration (Myr) | SFR ($10^{-6} M_{\odot} / \text{yr} / \text{arcmin}^2$) | HMXBs (Be-XRBs) | OB Stars | Pulsars |
| [1] | [2] | [3] | [4] | [5] | [6] | [7] | [8] | [9] |
| <i>Chandra</i> 3 | 00 56 46.14 | -72 18 10.78 | 66.8 | 68 | $44.04^{+10.07}_{-10.07}$ | 10 (7) | 2220 | 6 |
| <i>Chandra</i> 4 | 00 49 30.74 | -73 16 52.34 | 42.2 | 36 | $62.76^{+21.35}_{-20.83}$ | 17 (10) | 4060 | 8 |
| <i>Chandra</i> 5 | 00 53 11.45 | -72 26 29.92 | 42.2 | 28 | $81.86^{+13.89}_{-13.72}$ | 20 (16) | 2730 | 12 |
| <i>Chandra</i> 6 | 00 53 04.40 | -72 42 18.22 | 42.2 | 36 | $69.64^{+16.32}_{-10.76}$ | 20 (17) | 3040 | 12 |
| <i>Chandra</i> 7 | 00 49 25.00 | -72 44 22.80 | 26.6 | 30 | $54.51^{+25.35}_{-16.67}$ | 7 (6) | 1670 | 3 |
| <i>XMM-Newton</i> 1 | 01 07 52.00 | -72 53 41.60 | 10.6 | 8 | $35.30^{+26.88}_{-19.38}$ | 4 (0) | 3780 | 0 |
| <i>XMM-Newton</i> 2 | 00 51 56.63 | -72 02 53.20 | 16.8 | 15 | $15.66^{+17.83}_{-5.90}$ | 3 (2) | 3715 | 2 |
| <i>XMM-Newton</i> 3 | 00 42 25.45 | -73 36 29.40 | 66.8 | 39 | $15.65^{+6.47}_{-6.83}$ | 4 (0) | 1500 | 0 |
| <i>XMM-Newton</i> 6 | 00 40 05.19 | -72 47 57.40 | 668.3 | >1200 | $4.35^{+1.19}_{-0.99}$ | 0 (0) | 445 | 0 |

Note. — Columns 1-3: observed fields (ID, R.A., Decl.); Columns 4-6: age, duration -defined as the FWHM of its time evolution- and SFR; Columns 7-9: the number of HMXBs (Be-XRBs; see §2.1), OB stars (following Antoniou et al. 2009b), and pulsars (see §3).

Table 2. Properties of confirmed and candidate Be-XRBs detected with *XMM-Newton*

| Src | Source Name | R.A.(J2000.0) | Dec.(J2000.0) | Net | S/N | L_X^{un} | Optical | Off. (Unc.) | V | $B-V$ |
|------|-----------------|---------------|-------------------|-------------------------|--------------|--------------------|---|--------------------------|-----------------------|------------------------------|
| ID | XMMU J | (h m s) | ($^{\circ}$ ' ") | Counts | (σ) | (10^{34} erg/s) | src ID | (") | (mag) | (mag) |
| [1] | [2] | [3] | [4] | [5] | [6] | [7] | [8] | [9] | [10] | [11] |
| 1-1* | 010835.5-724308 | 01 08 35.54 | -72 43 08.4 | 63.87 ± 11.11 (1) | 5.75 | 2.79 ± 0.52 | O-11-104405 Z-4467654 | 3.82 (1.12) 3.73 | 17.82(2) 17.86(3) | -0.03(2) -0.04(4) |
| 1-2* | 010519.9-724943 | 01 05 19.90 | -72 49 43.1 | 18.83 ± 6.37 (3) | 2.96 | 2.22 ± 0.79 | O-10-78741 Z-4119599 | 3.73 (1.43) 4.01 | ... | ... ^a -0.09(4) |
| 1-3* | 010620.0-724049 | 01 06 20.01 | -72 40 49.1 | 33.98 ± 8.28 (3) | 4.10 | 5.45 ± 1.42 | O-10-118866 \equiv O-11-13325 Z-4232476 | 4.20 (1.59) 4.53 | 16.35(1) 16.38(3) | -0.02(2) 0.02(3) |
| 2-1 | 005255.1-715809 | 00 52 55.10 | -71 58 08.7 | 2155.48 ± 53.72 (2) | 40.12 | 135.75 ± 3.40 | Z-2430066 | 2.82 (0.10) ^b | 15.53(2) | -0.05(4) |
| 2-2* | 005149.3-720057 | 00 51 49.28 | -72 00 56.5 | 124.82 ± 16.09 (1) | 7.76 | 7.41 ± 0.96 | Z-2274521 | 3.46 (0.80) ^b | 18.38(3) | -0.01(5) |
| 3-1 | 004208.0-734502 | 00 42 08.01 | -73 45 01.9 | 214.72 ± 18.26 (1) | 11.76 | 14.22 ± 1.28 | O-2-79541 Z-1132154 | 0.59 (0.46) 0.40 | 16.78(2) 16.78(4) | -0.05(5) -0.10(8) |
| 3-2* | 004357.6-732840 | 00 43 57.57 | -73 28 39.7 | 24.56 ± 6.34 (2) | 3.87 | 2.63 ± 0.70 | O-3-122430 Z-1324298 | 0.65 (1.08) 0.57 | 18.31(2) 18.18(4) | -0.03(4) 0.12(5) |
| 3-3* | 004514.7-733601 | 00 45 14.73 | -73 36 00.7 | 23.25 ± 7.91 (1) | 2.94 | 1.69 ± 0.61 | O-3-178149 Z-1466431 | 2.73 (1.74) 2.62 | 15.17(1) 15.19(10) | -0.24(2) -0.23(11) |

Note. — Column 1: source ID as (field number)-(source ID in this field). Asterisks denote sources discovered within the *XMM-Newton* observations presented here); Column 2: source name; Column 3: right ascension. Column 4: declination; Column 5: number of net source counts (0.2-12.0 keV; EPIC camera-1=PN; 2=MOS1; 3=MOS2); Column 6: source significance; Column 7: absorption corrected X-ray luminosity (0.2-12.0 keV; see §2.1); Column 8: optical counterparts from OGLE-II as O-(field ID)-(source number) and MCPS as Z-(line number of the source in Table 1 of Zaritsky et al. 2002); Column 9: distance between the counterpart and the X-ray source (followed by the positional uncertainty of the X-ray sources given by the *edetect_chain* task); Columns 10-11: apparent V -band magnitude and $B - V$ color (with errors on the last significance digit).

^aDetected only in the B and I -bands: $B=16.87(1)$ mag, $I=16.76(2)$ mag.

^bThese offsets are within $2-3\sigma$ above the positional uncertainty, but the (R.A.,Decl.) separations are in the same direction indicating a boresight error, which however, cannot be corrected (§2.1).

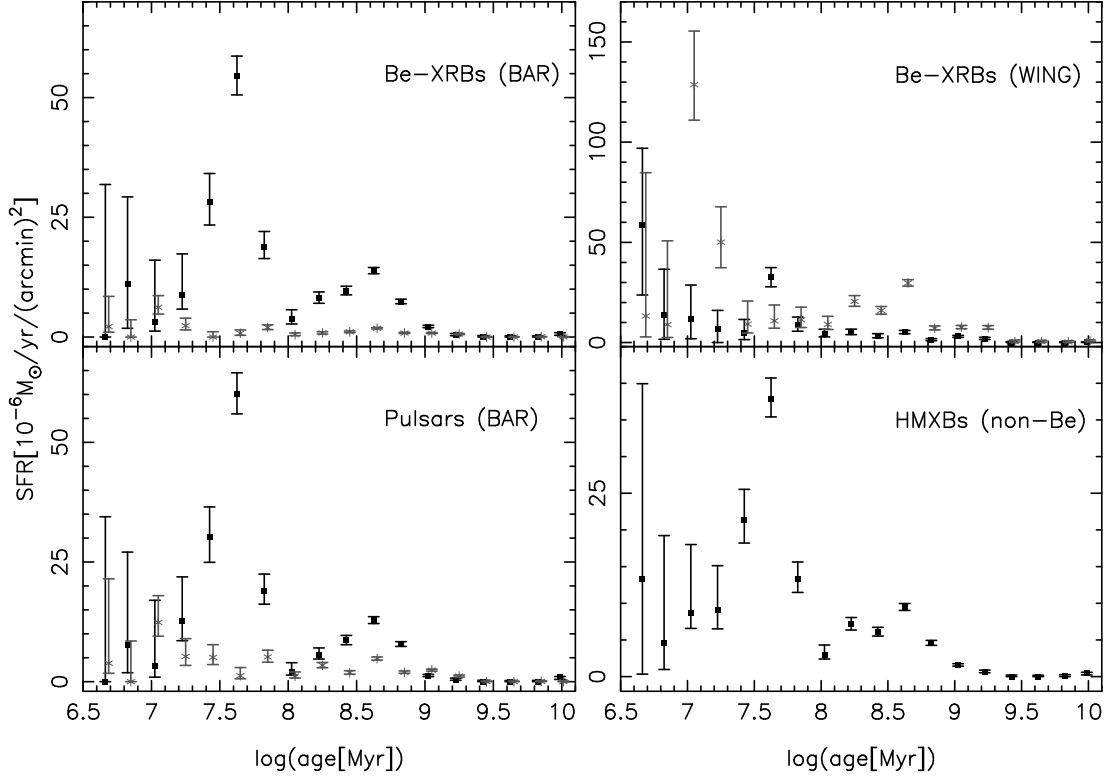


Fig. 1.— Average SFH (using data from [HZ04]) of regions with and without XRBs (black and gray points, respectively) in different locations of the SMC. *Top:* Be-XRBs in the Bar (*left*) and the Wing (*right*). *Bottom:* pulsars in the Bar (*left*) and HMXBs over the SMC (excluding spectroscopically confirmed Be-XRBs) from Liu et al. (2005; *right*). For clarity, a small offset of $\log(\text{age}[\text{Myr}]) \sim 0.025$ has been applied on the distributions to areas without Be-XRBs and/or pulsars.

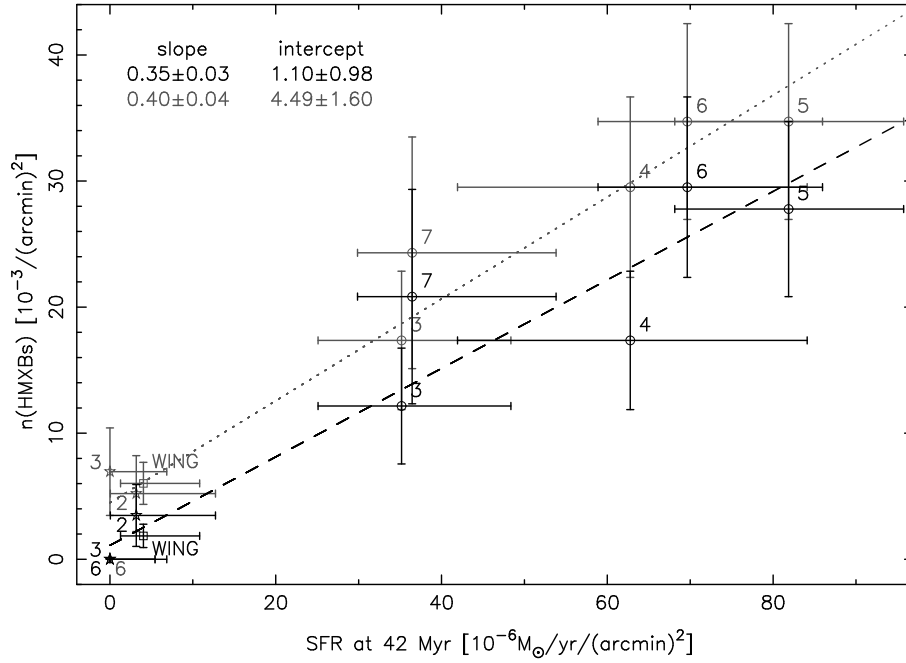


Fig. 2.— Number of observed Be-XRBs and HMXBs (shown in black and gray, respectively) in the *Chandra* and *XMM-Newton* fields vs. the SFR ~ 42 Myr ago. *Chandra* (circles) and *XMM-Newton* (asterisks) fields are marked with their IDs. The point marked as WING includes observations from *XMM-Newton* field 1 and fields 5487, 5490, 5494 and 5495 from the *Chandra* Wing survey (P.I. M. Coe).

Table 3. SFH of different X-ray source populations

| Region | Populations | Dominant SF Burst | | SFR | |
|----------|-------------------|-------------------|-------------------|---|-------------------------|
| | | Age | Duration (Myr) | of Most Intense Peak ($10^{-6} M_{\odot} / \text{yr} / (\text{arcmin})^2$) | at 42.2 Myr |
| [1] | [2] | [3] | [4] | [5] | [6] |
| SMC Bar | Be-XRBs | 42.2 | 33 | $54.50^{+4.16}_{-3.94}$ | $54.50^{+4.16}_{-3.94}$ |
| | Non Be-XRBs | 10.6 | 7 | $6.22^{+2.41}_{-1.44}$ | $0.78^{+0.71}_{-0.42}$ |
| SMC Bar | Pulsars | 42.2 | 33 | $60.09^{+4.43}_{-4.14}$ | $60.09^{+4.43}_{-4.14}$ |
| | Non Pulsars | 10.6 | 5 | $12.40^{+5.57}_{-2.90}$ | $1.25^{+1.70}_{-0.65}$ |
| SMC Wing | Be-XRBs | 4.6 | 8 | $58.47^{+38.48}_{-34.72}$ | $32.73^{+4.66}_{-4.91}$ |
| | | 42.2 ^a | 31 | $32.73^{+4.66}_{-4.91}$ | $32.73^{+4.66}_{-4.91}$ |
| | Non Be-XRBs | 10.6 | 25 | $128.69^{+26.73}_{-17.69}$ | $10.85^{+7.88}_{-3.69}$ |
| SMC Bar | Candidate Be-XRBs | 42.2 | 31 | $37.86^{+2.85}_{-2.45}$ | $37.86^{+2.85}_{-2.45}$ |

Note. — Column 1: SMC region; Column 2: source populations; Column 3: age of the most intense SF burst; Column 4: FWHM of burst’s time evolution; Column 5: SFR of most intense peak; Column 6: SFR at 42 Myr.

^aAdditional burst at ages <100 Myr.